Characterization of Cytoskeletal Pore Size Using Quantum Dots

Shuhuan Hu, Ya Liu, Chung Tin, and Raymond H. W. Lam

***Abstract*—Cytoskeletal pore size is a key factor in determining the intracellular molecular transportation, yet it is technically challenging to investigate correlations between the cytoskeletal pore size and cytoplasmic diffusion. Here, we report the application of quantum dots (QD) to measure the cytoskeletal pore size. QDs are first transfected into a cell, leading to different sizes of QD-encapsulating vesicles. The distribution of QD vesicles in cells reflects the cytoskeletal pore size. Further, we can predict the cytosolic viscosity from the measured pore size using the poroelasticity scaling theory. This predicted cytosolic viscosity is verified by measuring Brownian motions of the QDs in cells and transforming the motion characteristics into cytosolic viscosity via the Stocks–Einstein relation. This strategy also provides a practical method for quantifying the cytoskeletal pore sizes. Together, this research demonstrates the efficacy of applying QDs in further studies of intracellular physical properties that play key roles in intracellular molecular transports.**

***Index Terms*—Biological cells, biomedical imaging, elasticity, mesoporous materials, quantum dots.**

I. Introduction

CYTOSKELETON is an indispensable component of eukaryotic cells and plays a vital role in modulating a broad range of intracellular mechanistic activities [1]. Pathological features of cells have been shown to relate closely to abnormal behaviors of cytoskeleton in the contraction, deformation and other physical processes [2]. For example, the cytoskeletal structures and biophysical properties between normal and cancerous human epithelial cells are largely different [3]. It has been further demonstrated that cell stiffness can be applied for early diagnosis of cancer and the corresponding drug selection [4]. Though it has been well proven the correspondence between the stiffness and metastasis of cancer cells, the underlining mechanism remains largely elusive [5].

Recently, Moeendarbary *et al*. discovered that single cells behave like a poroelastic material [6]. The cytoskeleton can be considered as linear porous medium, in which interactions between fluid flow properties and the cytoskeletal deformation can be described by the poroelasticity theory. This may provide further explanations on the downstream biochemical responses mediated by the cytoskeletal architecture that cell deformation can trigger biochemical responses via poroelastic diffusion of intracellular molecules, which is determined by pore size and viscoelasticity of the cytoskeleton [7].

Technically, the cytoskeletal structures can be characterized by methods such as biochemical purification, immuno-fluorescence and atomic force microscopy [4]. On the other hand, the intracellular molecular movements can be traced by techniques such as electron spin resonance, and fluorescence recovery [8]. Nevertheless, there are still demands on the more comprehensive studies on relations between the cytoskeleton pore size and intracellular diffusion based on the cell poroelasicity.

In the past decade, quantum dots (QD) have been widely applied in bio-applications, especially intracellular imaging due to their extremely small particle size ($\sim$2–6 nm), biocompatibility and photobleaching resistance [9]. In particular, QDs have also been applied to visualize the intracellular molecular transport modulated by cytoskeleton [10]. Therefore, in this work we apply transfection of quantum dots (QD) [11] to human cells in order to examine the cytoskeletal pore size as well as the related scaling law of poroelasticity.

II. Methods

A. Cell Culture and Seeding

A green fluorescent protein (GFP)-transfected immortal cervical cancer cell line (GFP-Hela; Cell Biolabs Inc., San Diego, CA) was cultured in a high-glucose Dulbecco's modified Eagle's medium (DMEM; Invitrogen, Carlsbad, CA) with the supplement of 10% fetal bovine serum (Atlanta Biological, Atlanta, GA), 0.5 μg/mL fungizone (Invitrogen, Carlsbad, CA), 5 μg/mL gentamicin (Invitrogen), 100 units/mL penicillin, and 100 μg/mL streptomycin. The cells were maintained with 5% CO_2 in air at 37 °C and $\sim$100% humidity in an incubator.

Commercial biocompatible red quantum dots (Qtracker kit, red QD; Thermo Fisher Scientific, Carlsbad, CA) with diameters of 10–20 nm were used in the experiments. To transfect QD vesicles into cell cytosol, the labeling solution was prepared by a mixture of the growth medium, the QD crystal solution (10 nM) and the transfection reagent (0.5%, v/v), which is a cationic liposome formulation capable of encapsulating the QDs inside. During the subsequent incubation of 1 h, some QD vesicles were transfected into cell cytosol. The cells then continued to grow after replacing the labeling solution with the growth media for 1 day.

Afterward, we applied 0.25% trypsin-EDTA in phosphate buffered saline (PBS; Sigma-Aldrich, St. Louis, MO) to resuspend the QD-embedded GFP-Hela cells, following by centrifuge and replacement of fresh culture media. The cells were then seeded at a target cell density (6×10^3 cells/cm^2) in a confocal dish (#101350; SPL, Gyeonggi-do, Korea) coated with fibronectin (50 μg/mL in water, Sigma-Aldrich) for 2 h.

B. Imaging and Processing

After seeding the cells in the confocal dish, we applied a laser scanning confocal microscopy (TCS-SP8, Leica Microsystems, Wetzlar, Germany) with a 63 $\times$ oil immersion objective to capture high resolution (120 nm/pixel) time-lapse image stacks (z-spacing: 180 nm)

Manuscript received August 14, 2017; revised November 24, 2017; accepted November 30, 2017. Date of publication December 19, 2017; date of current version May 8, 2018. This work was supported by General Research Funds (Project# 124212 and 11206014) of Hong Kong Research Grant Council. *(Corresponding author: R. H. W. Lam.)*

S. Hu and Y. Liu are with the Department of Mechanical and Biomedical Engineering, City University of Hong Kong, Kowloon, Hong Kong (e-mail: shuhuanhu2-c@my.cityu.edu.hk; yaliu9-c@my.cityu.edu.hk).

C. Tin and R. H. W. Lam are with the Centre for Biosystems, Neuroscience, and Nanotechnology and the Department of Mechanical and Biomedical Engineering, City University of Hong Kong, Kowloon, Hong Kong, and also with the City University of Hong Kong Shenzhen Research Institute, Shenzhen 518057, China (e-mail: chungtin@cityu.edu.hk; rhwlam@cityu.edu.hk).

Digital Object Identifier 10.1109/TNANO.2017.2784962

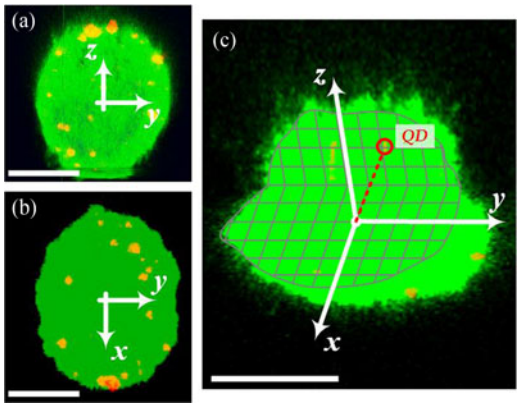

Fig. 1. (a) Side-view, (b) top-view and (c) isometric view of the same representative cell in a confocal dish for 7 min. The position of a QD inside a cell is identified by the Cartesian coordinates with an origin set as the volumetric center. For visualization, a portion of the cell body in the image stack was removed, with the cross-sections on the *x*-*y* and *y*-*z* planes represented with grids. A transfected QD inside the cell body is highlighted by the *red* circle. The cell body is in *green*; and the transfected QD are in *red*. Scale bars: 10 μm.

with a rate of 30 s/frame for 7 min. We adopted open source image processing software (ImageJ, National Institutes of Health) with a particle tracker plug-in (MosaicSuite) to process the microscopic image stacks. Limited by the computational capacity, we analyzed the *z*-projection images to observe the planar (2D) particle movement trajectory and quantified for the corresponding diffusion coefficient D_{2D}, instead of the three-dimensional (3D) motion. The 3D diffusion coefficient *D* could then be estimated by $D = 3/2 \times D_{2D}$.

III. Results and Discussion

A. Cytoskeletal Pore Size Reflected by QD Positions

Considering that the transport of QDs into cytoplasm was driven by transfection rather than the direct microinjection [6], the intake of QD vesicles [11] was dependent on the vesicle size. The QD vesicles larger than the cytoskeletal pores were physically blocked from further moving to the lower part of cytoplasm. During the observation period (7 min), the seeded cells were mostly with a spherical shape before their spreading on the surface as shown in Fig. 1(a). We also examined the perfect cell viability in our experiments using the live/dead viability testing kit (Thermo Fisher Scientific, Waltham, MA).

The position of each transfected QD can be represented by its distance from the cell centroid in *x*, *y* and *z*-directions [see Fig. 1(b)]. In this study, we have considered the dimensionless position ψ, which is defined by the QD-centroid distance relative to the cell radius *r*, i.e., $\psi = (x^2 + y^2 + z^2)^{1/2} / r$. For instance, a larger ψ should indicate a QD vesicle closer to the cortical region, whereas a smaller ψ (<0.7) reflects a QD vesicle inside the interior cytoskeletal mesh [12] and the cell nucleus often locates near the centroid ($\psi < 0.3$).

The volume of a QD vesicle *V* was measured by the total number pixels representing the vesicle volume, multiplying the single pixel volume (120 nm $\times$ 120 nm $\times$ 180 nm); and the vesicle size/diameter was computed by $d = (6V/\pi)^{1/3}$. Further, the circularity of the QDs was calculated by $(6V/\pi)/(D^3/2)^{3/2}$. The statistics of the vesicle size and circularity are shown in Fig. 2(a) and (b), respectively. The vesicles used in our experiments were fairly rounded (circularity: >0.75). Our result in Fig. 2(c) indicates that ψ should correlate with the size of the QD vesicle. This relation can be partially explained by the fact that

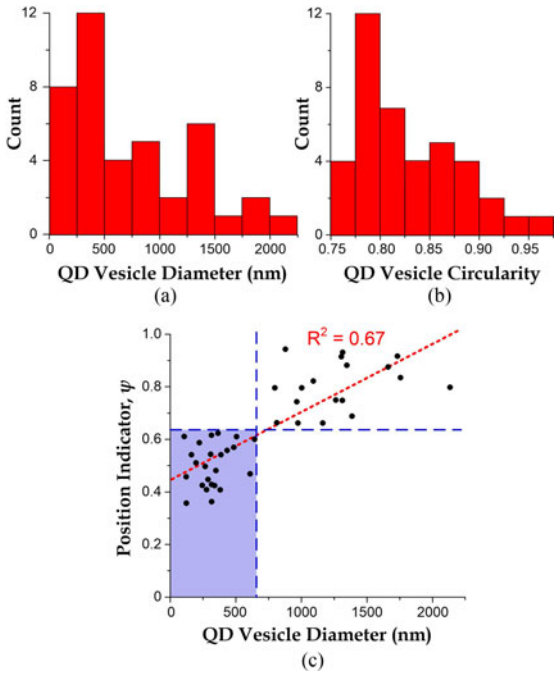

Fig. 2. Statistics of (a) QD vesicle diameter and (b) QD vesicle circularity. (c) Scatter plot of ψ and diameter of transfected QD vesicles, obtained from the results of 10 cells. The fitting line is in *red*; and QD vesicles in the cell interior fall in the *blue* region. QDs in 5 cells were summarized together.

smaller particles diffuse faster than the larger ones. More interestingly, the vesicles with a diameter smaller than ~500 nm consistently fall in the range of $\psi < 0.65$ (*blue* region in Fig. 2), suggesting that these smaller vesicle can move more freely within the cytoskeletal mesh. On the other hand, the vesicles larger than ~500 nm are only present in the cortical region. This critical vesicle diameter of ~500 nm should be a representative value for the cytoskeletal pore size, which agrees with possible range (450–5500 nm) as reported [13].

Collectively, these results provide meaningful insights about the intracellular transportation properties of the cells. Biophysical barriers including pores in the cytoskeletal mesh [8] are important factors in regulating intracellular vesicle transportation [7]. Our observation on the correlation between the vesicle sizes and the corresponding intracellular positions can be considered as direct evidence of the size effect in molecular transportation. Furthermore, molecular vesicles have been demonstrated to be an effective medium in intracellular signaling, drug delivery, metabolic regulation and molecular secretion [14]. The cytoskeletal pore size offers a hint for the appropriate vesicle size in the drug delivery applications.

B. Poroelastic Relation and QD Diffusivity

As the deformation of a poroelastic cell is resisted by both the elastic modulus of cytoskeleton and the viscosity of nanoscale infiltration flow of cytosol, the poroelasticity theory links macroscopic mechanical properties with microscopic structures of cytoskeleton and embedded liquids [15]. The poroelasticity of cells provides the insight of predicting their macroscopic biophysical properties by quantifying the microscopic intracellular structures, or *vice versa*. Actually, the whole cell viscosity is mainly contributed from the viscous flow of cytosolic infiltration; therefore the cytosolic viscosity can be estimated by the poroelastic scaling relation between the cytosolic viscosity μ and the

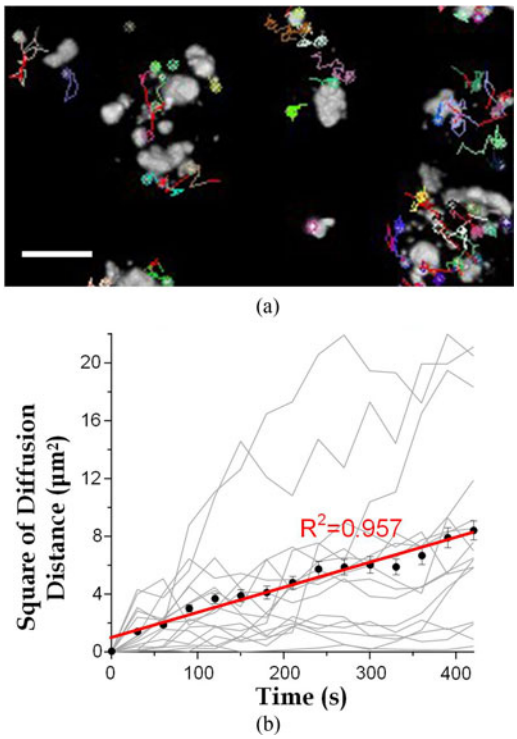

Fig. 3. (a) Trajectories of the QD vesicles with a diameter <360 nm embedded in cells. Each color line represents movement of a vesicle over 7 min of the cell seeding. The gray-scale micrograph is the QD distribution at the end of cell seeding. Scale bar: 8 μm. (b) Plot of square of the diffusion distance against diffusion time. The QD trajectories are selected from the same cell. The average distance squares at different time points are shown as *black* dots, with error bars representing the standard errors. The slope of the fitting line (*red*) reflects four times the planar diffusion coefficient ($= 4D_{2D}$) [13].

whole-cell viscosity η [6]:

$$\mu/\eta = \xi^2/D_{\text{cell}}^2 \tag{1}$$

where ξ ($\approx$500 nm as mentioned in the previous section) is the cytoskeletal pore size and $D_{\text{cell}} = 16.3 \pm \text{SE } 0.73\,\mu\text{m}$ is the diameter of the cell.

Recently, we have reported the measurement of whole-cell viscoelasticity by driving a cell along a confining microchannel such that the Young's modulus and viscosity of the cell can be converted from cell deformation based on the standard linear solid model and the Hertz and Tatara model [16]. We have applied this technique to obtain the viscoelastic properties of Hela cells, with whole-cell viscosity $\eta = 2.69 \pm \text{SE } 0.13$ kPa $\cdot$ s. Thus using Eqn. 1, the cytosolic viscosity could be obtained as $\mu = 2.7 \pm \text{SE } 0.3$ Pa $\cdot$ s.

In fact, this estimated cytosolic viscosity can be verified via observing the intracellular vesicle diffusion during the cell seeding period (7 min) in our experiments. Considering the diffusivity based on the Stocks-Einstein relation [17]:

$$D = k_B T/(3\pi\mu D_{\text{QD}}) \tag{2}$$

where $k_B = 1.38 \times 10^{-23}$ J/K is the Boltzmann constant; $T = 310$ K is the absolute temperature; μ is the cytosol viscosity and D_{QD} is the diameter of the vesicle. To obtain the cytosolic viscosity μ of the Hela cells, we performed time-lapse confocal scans for the QD positions throughout the cell seeding period (7 min) to obtain the cytosolic diffusion coefficient *D*. Trajectories of the QDs were analyzed using commercial software as shown in Fig. 3(a). Notably, only QD vesicles with a sufficiently small diameter ($\sim$120–240 nm) were analyzed such that the barrier effects by the cytoskeletal mesh were negligible. The planar diffusivity D_{2D} was analyzed based on the intracellular Brownian motion governed by the Fick's second law that squares of the diffusion length should increase with time. Therefore, D_{2D} was obtained as the slope of a linear-fitting line for the plot of squares of diffusion distance against time as shown in Fig. 3(b). Next, we can convert this value to the 3D diffusivity $D\,(= 3/2 \times D_{2D} = 0.0013 \pm \text{SE } 0.0002\,\mu\text{m}^2/\text{s}$, averaged from values of 10 cells). Using Eqn. (2) and subsidizing the diffusivity value as well as assuming an average vesicle diameter $D_{\text{QD}} = 180$ nm, the cytosolic viscosity could be obtained as $2.4 \pm \text{SE } 0.3$ Pa $\cdot$ s, indicating a reasonable agreement with the value estimated based on the pore size and the poroelasticity relation ($2.7 \pm \text{SE } 0.3$ Pa $\cdot$ s). Importantly, if we reconsider such 3D diffusivity for the 1-day cell culture duration before the measurement, the diffusion distance (>20 μm) of the largest vesicles (2000 nm in diameter) is longer than the cell diameter. Thus, the larger vesicles (>500 nm) occurred in the cortical region were blocked by the interior cytoskeletal mesh rather than the smaller molecular diffusivity.

The minor difference between then measured cytosolic viscosity μ and the estimated value using the poroelasticity relation might result from the hypothesis of causation of the biophysical properties. The adopted poroelasticity theory assumes that only the interstitial flow of the cytosol contributes to the viscosity. However, other factors such as minor blockage of the cytoskeleton, repeated breakages and reforms of weak bonds around the fibers partially can contribute to a higher viscosity [18]; and hence the measured cytosolic viscosity ($\sim$2.4 Pa·s) is slightly smaller than the prediction based on the poroelasticity scaling relation (2.7 Pa·s).

This result also indicates that we can convert the measured *D* to predict the cytoskeletal pore size according to the poroelasticity theory. Using again Eqn. (1), we can obtain an estimate of the cytoskeletal pore size as 478 ± 73 nm, which is comparable to the values measured by high resolution fluorescent imaging ($\sim$400 nm [19]) and electron imaging (200–1000 nm [4], [7]). Although the measurement based on the distribution of QD positions described in the last section is more straightforward, it can only induce a range of the possible pore size. Calculating the cytoskeletal pore size based on the Brownian motion of QD encapsulated vesicles and the poroelasticity scaling relation provides a more insightful value than the observation of static blockage because such measurement links the transportation dynamics of vesicles, which is also crucial for governing cell functions.

IV. Conclusion

We presented the measurement of cytoskeletal pore size using QD vesicles. Various sizes of vesicle encapsulated QDs inside cell were accomplished by transfection. High-resolution 3D confocal scans of GFP-Hela cells were performed for visualizing the QD positions during the cell seeding process. The cytoskeletal pore size was revealed based on the distribution of vesicle positions and sizes; whereas the cytosolic diffusivity could be observed by the Brownian motion of vesicles in cells according to the Stock-Einstein relation. Importantly, we have proven that the cytoskeletal pore size and the cytosolic diffusivity are related by a poroelastic scaling relation. Our results further demonstrated that these two cell properties are interchangeable with very good agreements (<10% deviations between the measured value and the estimated values based on the poroelasticity theory). In summary, our method of QD-based cytoskeletal pore size measurement can be applied together with other standard cell analysis techniques to further unveil important roles of intracellular transportation in mechanistic studies. Additionally, this

study provides insights on drug design, including the relation between size and position of drug-encapsulated vesicles in cells, for configuring the effective vesicle size and dosage inducing more effective treatment results.

REFERENCES

[1] D. A. Fletcher and R. D. Mullins, "Cell mechanics and the cytoskeleton," *Nature*, vol. 463, no. 7280, pp. 485–492, 2010.

[2] M. Malacombe, M.-F. Bader, and S. Gasman, "Exocytosis in neuroendocrine cells: New tasks for actin," *Biochim. Biophys. Acta, Mol. Cell Res.*, vol. 1763, no. 11, pp. 1175–1183, 2006.

[3] A. N. Ketene, E. M. Schmelz, P. C. Roberts, and M. Agah, "The effects of cancer progression on the viscoelasticity of ovarian cell cytoskeleton structures," *Nanomedicine, Nanotechnol. Biol. Med.*, vol. 8, no. 1, pp. 93–102, 2012.

[4] S. E. Cross, Y.-S. Jin, J. Rao, and J. K. Gimzewski, "Nanomechanical analysis of cells from cancer patients," *Nature Nanotechnol.*, vol. 2, no. 12, pp. 780–783, 2007.

[5] S. Suresh *et al.*, "Reprint of: Connections between single-cell biomechanics and human disease states: Gastrointestinal cancer and malaria," *Acta Biomater.*, vol. 23, pp. S3–S15, 2015.

[6] E. Moeendarbary *et al.*, "The cytoplasm of living cells behaves as a poroelastic material," *Nature Mater.*, vol. 12, no. 3, pp. 253–261, 2013.

[7] I.-M. Yu and F. M. Hughson, "Tethering factors as organizers of intracellular vesicular traffic," *Annu. Rev. Cell Develop. Biol.*, vol. 26, pp. 137–156, 2010.

[8] G. T. Charras, T. J. Mitchison, and L. Mahadevan, "Animal cell hydraulics," *J. Cell Sci.*, vol. 122, no. 18, pp. 3233–3241, 2009.

[9] X. Michalet *et al.*, "Quantum dots for live cells, in vivo imaging, and diagnostics," *Science*, vol. 307, no. 5709, pp. 538–544, 2005.

[10] E. A. Katrukha *et al.*, "Probing cytoskeletal modulation of passive and active intracellular dynamics using nanobody-functionalized quantum dots," *Nature Commun.*, vol. 8, pp. 1–8, 2017.

[11] X. Nan, P. A. Sims, P. Chen, and X. S. Xie, "Observation of individual microtubule motor steps in living cells with endocytosed quantum dots," *J. Phys. Chem. B*, vol. 109, no. 51, pp. 24220–24224, 2005.

[12] R. G. Fehon, A. I. McClatchey, and A. Bretscher, "Organizing the cell cortex: The role of ERM proteins," *Nat. Rev. Mol. Cell Biol.*, vol. 11, no. 4, pp. 276–287, 2010.

[13] P. Saffman and M. Delbrück, "Brownian motion in biological membranes," *Proc. Nat. Acad. Sci. USA*, vol. 72, no. 8, pp. 3111–3113, 1975.

[14] T. Hayashi, J. F. Wojtaszewski, and L. J. Goodyear, "Exercise regulation of glucose transport in skeletal muscle," *Amer. J. Physiol. Endocrinol. Metabolism*, vol. 273, no. 6, pp. E1039–E1051, 1997.

[15] S. Hu *et al.*, "Multiparametric biomechanical and biochemical phenotypic profiling of single cancer cells using an elasticity microcytometer," *Small*, vol. 12, pp. 2300–2311, 2016.

[16] S. Hu and R. H. Lam, "Characterization of viscoelastic properties of normal and cancerous human breast cells using a confining microchannel," *Microfluid. Nanofluid.*, vol. 21, no. 4, pp. 82–92, 2017.

[17] J. Brillo, A. I. Pommrich, and A. Meyer, "Relation between self-diffusion and viscosity in dense liquids: New experimental results from electrostatic levitation," *Phys. Rev. Lett.*, vol. 107, no. 16, 2011, Art. no. 165902.

[18] B. D. Hoffman, C. Grashoff, and M. A. Schwartz, "Dynamic molecular processes mediate cellular mechanotransduction," *Nature*, vol. 475, no. 7356, pp. 316–323, 2011.

[19] T. Kiuchi, M. Higuchi, A. Takamura, M. Maruoka, and N. Watanabe, "Multitarget super-resolution microscopy with high-density labeling by exchangeable probes," *Nature Methods*, vol. 12, no. 8, pp. 743–746, 2015.